Cell

A Code for RanGDP Binding in Ankyrin Repeats Defines a Nuclear Import Pathway

Min Lu,[1] Jaroslav Zak,[1] Shuo Chen,[1] Luis Sanchez-Pulido,[2] David T. Severson,[1] Jane Endicott,[3] Chris P. Ponting,[2] Christopher J. Schofield,[4] and Xin Lu[1,*]
[1]Ludwig Institute for Cancer Research, Nuffield Department of Clinical Medicine, University of Oxford, Oxford, OX3 7DQ, UK
[2]MRC Functional Genomics Unit, Department of Physiology Anatomy and Genetics, University of Oxford, Oxford, OX1 3PT, UK
[3]Northern Institute for Cancer Research, University of Newcastle, Newcastle, NE2 4HH, UK
[4]Chemistry Research Laboratory, Department of Chemistry, University of Oxford, Oxford, OX1 3TA, UK
*Correspondence: xin.lu@ludwig.ox.ac.uk
http://dx.doi.org/10.1016/j.cell.2014.05.006

SUMMARY

Regulation of nuclear import is fundamental to eukaryotic biology. The majority of nuclear import pathways are mediated by importin-cargo interactions. Yet not all nuclear proteins interact with importins, necessitating the identification of a general importin-independent nuclear import pathway. Here, we identify a code that determines importin-independent nuclear import of ankyrin repeats (ARs), a structural motif found in over 250 human proteins with diverse functions. AR-containing proteins (ARPs) with a hydrophobic residue at the 13th position of two consecutive ARs bind RanGDP efficiently, and consequently enter the nucleus. This code, experimentally tested in 17 ARPs, predicts the nuclear-cytoplasmic localization of over 150 annotated human ARPs with high accuracy and is acquired by the most common familial melanoma-associated *CDKN2A* mutation, leading to nuclear accumulation of mutant p16ink4a. The RaDAR (RanGDP/AR) pathway represents a general importin-independent nuclear import pathway and is frequently used by AR-containing transcriptional regulators, especially those regulating NF-κB/p53.

INTRODUCTION

Nuclear transport of macromolecules is a fundamental biological process lying at the heart of eukaryotic gene expression and cell fate determination. The nuclear import of large molecules (>~40 kDa) and/or the accumulation of small molecules against a concentration gradient requires facilitated transport (Adams and Wente, 2013; Mohr et al., 2009). Most established facilitated transport mechanisms are mediated by nuclear transport proteins called karyopherin-βs (Kap-βs, also known as importins and exportins in humans) (Görlich and Kutay, 1999; Stewart, 2007; Weis, 2003). Eleven of 19 known Kap-βs are involved in nuclear import (Chook and Süel, 2011). The best-characterized nuclear import process is mediated by importin-cargo interactions in which importins (importins 2-5, 7-9, 11-13 and exportin 4) interact with nuclear localization signal (NLS)-containing cargos. The resulting importin-cargo complex interacts with phenylalanine-glycine repeat containing nucleoporins (FG-Nups) to pass through the nuclear pore complex (NPC). A prerequisite of this important system is the asymmetric distribution of RanGDP and RanGTP between the cytoplasm and nucleus. The cytoplasm has relatively high RanGDP levels, gained through the activity of the cytoplasmic RanGTPase-activating protein (RanGAP). In the nucleus, RanGDP is converted to RanGTP by nuclear Ran guanine nucleotide exchange factor (RCC1). The high nuclear concentration of RanGTP enables it to compete with the cargos to bind importin, thus enabling release of NLS-containing cargos into the nucleoplasm.

The formation of the RanGTP/importin-β complex accompanies the termination of nuclear import, followed by recycling of importins and RanGTP to the cytoplasm (Kutay et al., 1997; Stewart, 2007). RanGTP is also exported to the cytoplasm by coupling to the exportin-mediated nuclear export pathway. Despite of the continuous nuclear export of RanGTP, >90% of Ran resides in the nucleus, which cannot be achieved by passive diffusion (Kim and Elbaum, 2013). This has led to the identification of nuclear transport factor 2 (NTF2) as an important nuclear import facilitator of RanGDP (Ribbeck et al., 1998). NTF2-mediated nuclear import of RanGDP is a continuous and extremely efficient event. The low-energy GDP form of Ran has historically been viewed as the "off" state because it does not directly participate in various identified nuclear import/export pathways (Cook et al., 2007), and the function of RanGDP in nuclear-cytoplasmic transport has not yet been identified. Interestingly, the actin-associated protein CapG is reported to bind NTF2 to achieve nuclear entry with the assistance of Ran and Nup62 (Van Impe et al., 2008). Thus, a key question is whether the extremely efficient NTF2-RanGDP import pathway can be used by other cargos as a facilitated nuclear import pathway.

While the best-characterized nuclear import pathways are mediated by importin-NLS-containing cargo interactions, many nuclear proteins do not contain a currently identifiable NLS (Chook and Süel, 2011). A bioinformatics study shows that only 60% of the nuclear proteome contain identifiable NLS sequences (Brameier et al., 2007). Additionally, the importin-independent pathways that have been identified to date tend to be cargo specific. For example, nuclear import of

Hsp70s-ATP is mediated by Hikeshi (Kose et al., 2012); CapG is mediated by NTF2/Ran/Nup62 (Van Impe et al., 2008); β-catenin is mediated by direct nucleoporin binding (Fagotto et al., 1998); and RanGDP is mediated by NTF2 (Ribbeck et al., 1998). Collectively, these observations imply the presence of at least one general nuclear import system that is independent of importins.

Intriguingly, a number of ankyrin repeat domains (ARDs), such as those from IκBα, ASPP2, and GABPβ, have been reported to enter the nucleus via an unknown mechanism independent of a NLS (Sachdev et al., 1998). The ankyrin repeat (AR) is one of the most common protein structural motifs. To date, >265 human proteins are annotated as AR-containing proteins (ARPs) in the SMART database. ARs are evolutionarily conserved protein modules, of ~33 residues and an L-shaped structure, composed of two antiparallel α helices of 8–10 residues preceded by a β-hairpin. The Ankyrin family is one of the most representative ARP families. Its members (AnkyrinR/B/G) are adaptor proteins that mediate the attachment of integral membrane proteins to the spectrin-actin-based membrane cytoskeleton (Bennett and Baines, 2001), thus ARPs are often thought of as scaffold proteins. However, ARPs also play pivotal roles in the development and maintenance of tissue homeostasis by functioning at the cell membrane, cytoplasm, and nucleus. Some ARPs interact with their ligands with nanomolar affinity and high specificity, forming the basis of synthetic AR-based "alternative antibodies" (such as DARPin), which efficiently target binding partners (Dreier et al., 2013).

Mutations in the ARDs of ARPs have been associated with various human diseases. For example, mutations in AnkyrinR and AnkyrinB correlate with hereditary spherocytosis (Eber et al., 1996) and cardiac arrhythmia (Mohler et al., 2003), respectively. Recent studies also suggest their importance in tumorigenesis. The ARD of Notch is mutated in human lung and head and neck cancers (Agrawal et al., 2011). The most frequent $p16^{ink4a}$ (p16, encoded by *CDKN2A*) mutation in human familial melanomas is methionine to isoleucine at residue 53 (M53I), resulting in the nuclear enrichment of p16 (Ghiorzo et al., 2004). It remains unknown why a point mutation in p16 can facilitate its nuclear localization. The importance of ARP localization in tumorigenesis is further supported by recent discoveries of how the ASPP protein family functions. The ASPP family was originally identified as transcriptional regulators of p53 (Samuels-Lev et al., 2001) and RelA/p65 (Yang et al., 1999), and consists of three members (ASPP1, ASPP2, and iASPP) that shuttle between the cytoplasm and nucleus. ASPP1 binds YAP and acts as an oncogene in the cytoplasm (Vigneron et al., 2010) but acts as a tumor suppressor in the nucleus by enhancing p53-mediated apoptosis (Aylon et al., 2010). In the cytoplasm, ASPP2 binds Ras and inhibits autophagy (Wang et al., 2013). ASPP2's N terminus also binds Par3 to maintain the integrity of apical polarity and tight junctions (Sottocornola et al., 2010). In the nucleus, ASPP2 is a transcriptional activator of the p53 family and a tumor suppressor that co-operates with p53 to suppress tumor growth in vivo (Vives et al., 2006). Similarly, iASPP is a nuclear protein in proliferating basal epithelial cells but cytoplasmic in differentiated epithelial cells in human cervical or skin epithelia in vivo (Notari et al., 2011). During G_2/M transition, cyclin B/CDK1 phosphorylates Ser84 and Ser113 of iASPP, resulting in its nuclear entry and enhanced inhibition of p53 (Lu et al., 2013). Deregulation of Ser84 and Ser113 phosphorylation is a key reason for the loss of p53's tumor suppressive function in human melanoma. These findings demonstrate the importance of the cellular localizations of ASPP in regulating their functions. However, little is known about the mechanisms mediating their nuclear entry, except for observations that, like IκBα, ASPP2's ARD and the ARD and SH3-containing C terminus of iASPP can enter the nucleus without an identifiable NLS in vitro (Sachdev et al., 1998; Slee et al., 2004). Here, we reveal that a group of ARDs possess a protein code, consisting of hydrophobic residues at the 13th position of the consensus AR sequences in two consecutive ARs to form a 3D-binding motif for RanGDP binding, which mediates nuclear entry. Thus, the *Ran*G*DP*/*AR* (RaDAR) complex-mediated nuclear import system represents a general importin-independent nuclear import pathway.

RESULTS

ARs of ASPP Enter the Nucleus via an Importin-Independent Pathway

Increased cytoplasmic GTP concentration inhibits importin-dependent nuclear import because elevated RanGTP in the cytoplasm prevents NLS-containing proteins from interacting with importins (Melchior et al., 1993). Thus, the ability of cytoplasmic GTP or GTPγS (a nonhydrolyzable GTP analog that cannot supply energy) to influence nuclear entry in a digitonin-permeabilized in vitro nuclear import assay may indicate whether a protein employs the importin-dependent or an independent pathway to enter the nucleus.

Recombinant GST-tagged ARs from iASPP and ASPP2, iASPP-ARs-GST, and ASPP2-ARs-GST (Figure S1A available online) were purified and their ability to enter the nucleus compared with GST-tagged NLS-GFP (NLS-GFP-GST), which contains the SV40 NLS sequence (Figure 1A). FITC-labeled ASPP-ARs-GST and NLS-GFP-GST entered the nucleus efficiently when loaded onto digitonin-treated cells. Under the same conditions, FITC-labeled GST did not enter the nucleus (Figure S1B). The presence of GTP or GTPγS abrogated NLS-GFP-GST's nuclear entry; in contrast they enhanced the nuclear entry of ASPP-ARs-GST (Figure 1A). To our knowledge, RanGDP is the only protein whose nuclear import can be enhanced by the addition of GTP (Ribbeck et al., 1998), as confirmed here (Figure 1A).

The ability of ASPP-ARs-GST to interact with key components of the well-defined classical nuclear import pathway was then further investigated. As expected, NLS-GFP-GST pulled down importin-α, whereas GST-RanGDP pulled down Ran-binding domain-containing Nup358 and Nup153 (Figures 1B and S1C). Under the same conditions, ASPP-ARs-GST failed to complex with FG-Nups Nup358, Nup214, Nup98, or Nup62, which span the NPC. This may be due to the fact that interactions between transport complexes and FG-repeats are transient with a low affinity. However, FG-Nup Nup153, which resides at the nuclear ring of NPC, interacted with ASPP-ARs-GST, NLS-GFP-GST, and GST-RanGDP. ASPP-ARs-GST pulled down Ran as well as NTF2 (Figure 1B).

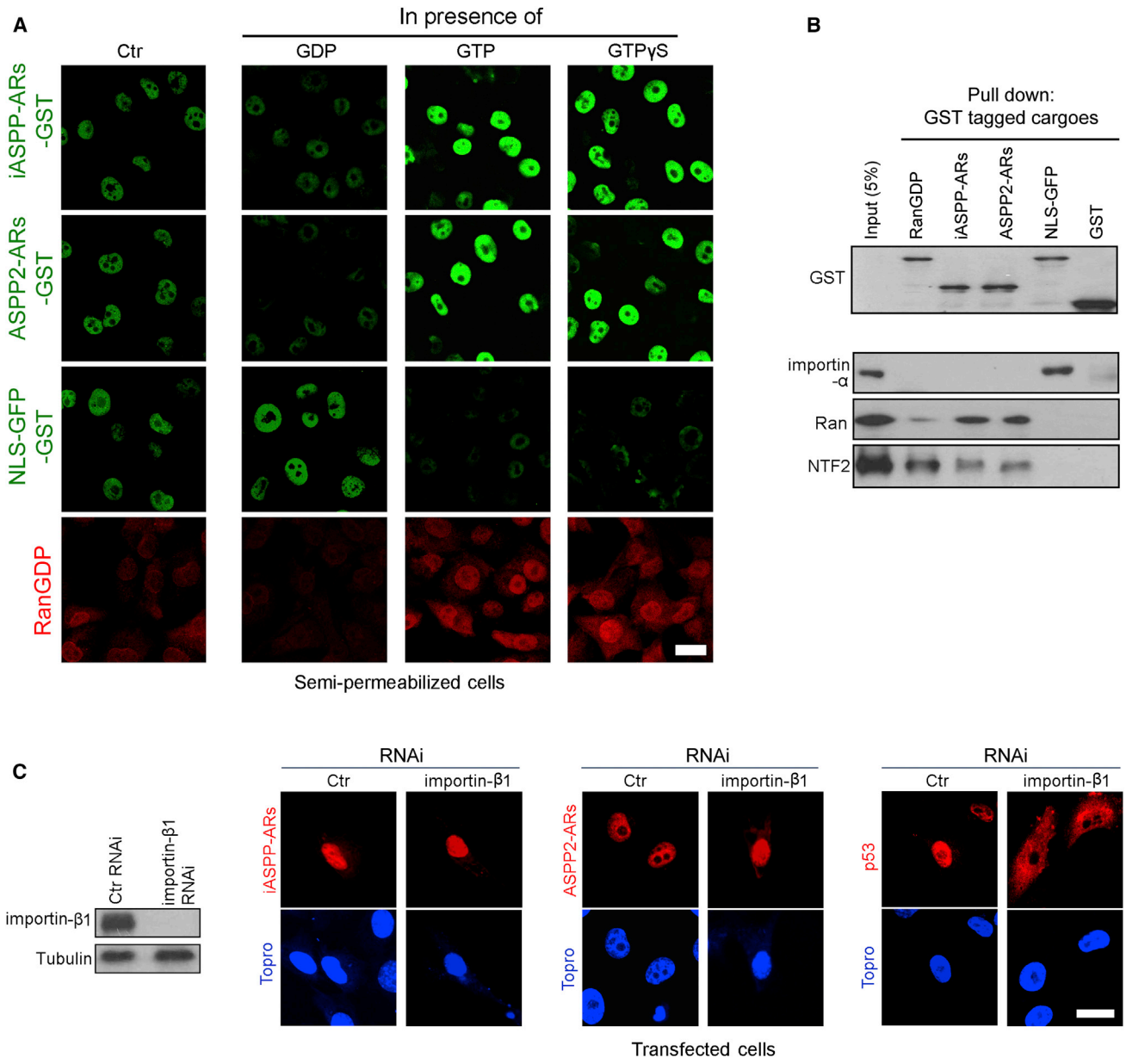

Figure 1. Nuclear Import of ASPP-ARs via an Importin-Independent Pathway

(A) Digitonin-treated semipermeable H1299 cells were incubated with FITC-labeled substrates (purified ASPP-ARs-GST or NLS-GFP-GST) in the presence of 10 mg/ml H1299 cytosol and an energy-regenerating mixture in NIP buffer. In right 3 panels, 2 mM GDP, GTP, or GTPγS was added. Cellular localization of the substrates was determined by direct FITC fluorescence observation. Ran freshly loaded with GDP was labeled with PE (red) and used as a control. Scale bar, 20 μm.

(B) 5 μg indicated purified GST-tagged proteins were bound on glutathione beads and incubated in 2 mg/ml H1299 cell lysates for 2 hr at room temperature (RT), followed by washes and immunoblotting.

(C) Control (Ctr) or importin-β1 RNAi was transfected in H1299 cells for 24 hr, followed by ASPP-ARs-V5 or p53 transfection for another 48 hr. Cellular localizations of transfected proteins and importin-β expression were determined. Scale bar, 20 μm.

See also Figure S1.

To provide further evidence that ASPP-ARs can enter the nucleus via an importin-independent pathway, importin-β1 was knocked-down in H1299 cells before transfection with ASPP-ARs or p53 (contains a NLS). While knockdown of importin-β1 impaired p53's nuclear accumulation, it had a minimal effect on the nuclear accumulation of ASPP-ARs (Figure 1C). These results suggest that ASPP-ARs can enter the nucleus independently of importins.

ASPP-ARs Directly Bind RanGDP and Form an AR/RanGDP/NTF2 Complex to Mediate Nuclear Entry

Since RanGDP continuously enters the nucleus via NTF2, we tested whether ASPP-ARs could employ RanGDP to enter the nucleus. ASPP-ARs-GST or GST was incubated with purified RanGDP (freshly loaded GDP) in a GST pull-down assay. Direct interaction between RanGDP and ASPP-ARs-GST, but not GST, was observed (Figure 2A). The ARs-containing fragment (622-757) mediated the observed interaction between iASPP and RanGDP (Figure S2A).Previous studies imply that ARs bind their partners in a manner where the ARs adopt a canonical tertiary structure as observed in multiple crystal structures (Sedgwick and Smerdon, 1999). By far-western dot blot assay, we observed that only native ASPP-ARs-GST, and not urea-denatured ASPP-ARs-GST, interacted with RanGDP (Figure 2B, left). As a positive control, the membrane was incubated with an anti-GST antibody that detects the presence of both native and denatured ASPP-ARs-GST. Denaturation has minimal impact on the signals detected (Figure 2B, right). Furthermore, ASPP-ARs-GST failed to directly interact with FG-Nups (FxFG, GLFG, SxFG, or PxFG) that are known to be involved in the classical nuclear import pathway. NTF2's interaction with FxFG-containing Nup153 acted as a positive control (Figure S2C) (Morrison et al., 2003). These data suggest that ASPP-ARs bind RanGDP directly in a tertiary structure-dependent manner, and that the observed interaction with Nup153 in cell lysates may be mediated by RanGDP/NTF2.

When NTF2 binds RanGDP, the resulting NTF2/RanGDP complex enters the nucleus more efficiently than RanGDP alone (Ribbeck et al., 1998). Although iASPP-ARs-GST was able to bind RanGDP, it failed to interact directly with NTF2. However, it did pull down NTF2 in the presence of RanGDP. In addition, iASPP-ARs failed to pull down NTF2(E42K), a mutant defective in RanGDP binding, in the presence of RanGDP. Interestingly, iASPP-ARs-GST did not bind RanGTP under the same conditions (Figure 2C).

In an in vitro nuclear import assay, incubation of FITC-labeled iASPP-ARs-GST together with BSA detected nuclear iASPP-ARs-GST in 89% of cells. Only ~14% of the cells contained a strong nuclear iASPP-ARs-GST signal (saturated FITC, red in heat map, Figures 2D and S2D). However, in the presence of RanGDP, ~45% of cells manifested strong nuclear iASPP-ARs-GST (Figure 2D and Figure S2D). Cells with nuclear RanGDP were clearly associated with stronger nuclear iASPP-ARs-GST signals (Figure 2D, arrowheads, enlarged panel). Similar enhancement upon RanGDP addition was observed for ASPP2-ARs-GST, but not NLS-GFP-GST, implying that RanGDP nuclear import is specifically employed by ASPP-ARs. Ran(Q69L)GTP, a dominant-negative mutant of Ran that is locked in a GTP-bound form and defective in nuclear import, reduced the percentage of strong nuclear iASPP-ARs-GST-manifesting cells to <15%. Ran-GFP overexpression in H1299 cells induced stronger nuclear iASPP localization, while Ran(Q69L)-GFP failed to do so (Figure 2E).

Incubation of iASPP-ARs-GST with RanGDP in the presence of NTF2 enhanced the nuclear iASPP-ARs-GST signal, whereas NTF2(E42K) did not (Figure S2D). These results demonstrate that the ASPP-ARs bind RanGDP directly, forming a protein complex with NTF2 via RanGDP that enables their nuclear entry.

RanGDP Binds Hydrophobic 13th Residues of ARs and Mediates Nuclear Import

The NPc (nucleophosmin core, a predominantly cytoplasmic protein)-fused second AR of IκBα (NPc-IκBα-AR2) was previously shown to locate in the nucleus (Sachdev et al., 1998). However, NPc-IκBα-AR2(AAA), a mutant with triple alanine substitutions on the 8th, 10th, and 13th residues of the AR, located in the cytoplasm. Interestingly, NPc-IκBα-AR2 bound RanGDP more strongly than NPc-IκBα-AR2(AAA) (Figure S3A). As NPc-IκBα-AR2 contains only one AR, this provided an opportunity to identify the specific AR residues that mediate RanGDP interaction. Previous studies have shown that ARs most commonly interact with their binding partners via residues located on the AR grooves, composed of the 3rd–15th residues in the AR consensus sequence (Figure 3A, star line) (Sedgwick and Smerdon, 1999). The start position of an AR is defined according to common structural folds (Figure 3A). As RanGDP only binds natively folded ASPP-ARs, the residues that maintain the AR's tertiary structure (Figure 3A, triangles; according to studies on the artificial consensus AR) (Kohl et al., 2003) were not mutated. Based on a crystal structure of IκBα's ARs (PDB accession code: 1NFI), the 3rd, 5th, 13th, and 14th residues, which would not affect AR structure but are located on the AR grooves, were mutated to generate NPc-IκBα-AR2 (L114A, Q116A, I124A, and T125A), respectively. Interestingly, only NPc-IκBα-AR2 (I124A, position 13) weakened RanGDP binding (Figure S3B). In the tertiary structure, the 13th AR residue (AR_{13}) is located at the end of the first α-helix (at the upper tip of the groove) and is exposed, extending out of the AR (Figure 3A, red stars).

Within the UniProt Human Reviewed ARPs, the occurrence of amino acids at the 13th positions of human ARs is biased toward R, S, Q, and A (Figure S3B). Thus, AR_{13} of NPc-IκBα-AR2, I124, was substituted individually with the ten most frequently occurring amino acid residues (accounting for 79% of ARPs). The resulting IκBα-AR2 mutants with hydrophobic AR_{13} (I124I, I124L, I124F, and I124C) all bound RanGDP with high efficiency, whereas mutants with more hydrophilic residues at AR_{13}, K or R, bound RanGDP with much lower efficiency (Figure 3B). Consistent with RanGDP-binding affinity, strong RanGDP-binding NPc-IκBα-AR2s (WT, I124L and I124F) were mainly observed in the nucleus, whereas weaker mutants (NPc-IκBα-AR2[124R and 124K]) were predominantly cytoplasmic (Figure 3B).

ANKRD49 is predominantly cytoplasmic with four ARs, and RanGDP binding is barely detectable. None of the four AR_{13}s of ANKRD49 (E, Y, K, and G) belongs to the highly hydrophobic residues. They were thus substituted for the more hydrophobic I and C, which occur at position 13 of the ARs of IκBα and iASPP, respectively. Interestingly, a point substitution to replace the existing Y or K to I or C, at AR_{13} of the second or third ARs, achieved a small but detectable increase in RanGDP binding. When two or more AR_{13} in consecutive ARs were substituted for C (E-C-C-G or E-C-C-C), RanGDP binding was significantly increased (Figure 3C), resulting in enhanced nuclear localization. In addition, ANKRD49 mutants with hydrophobic AR_{13} in two consecutive ARs were more active in binding RanGDP and

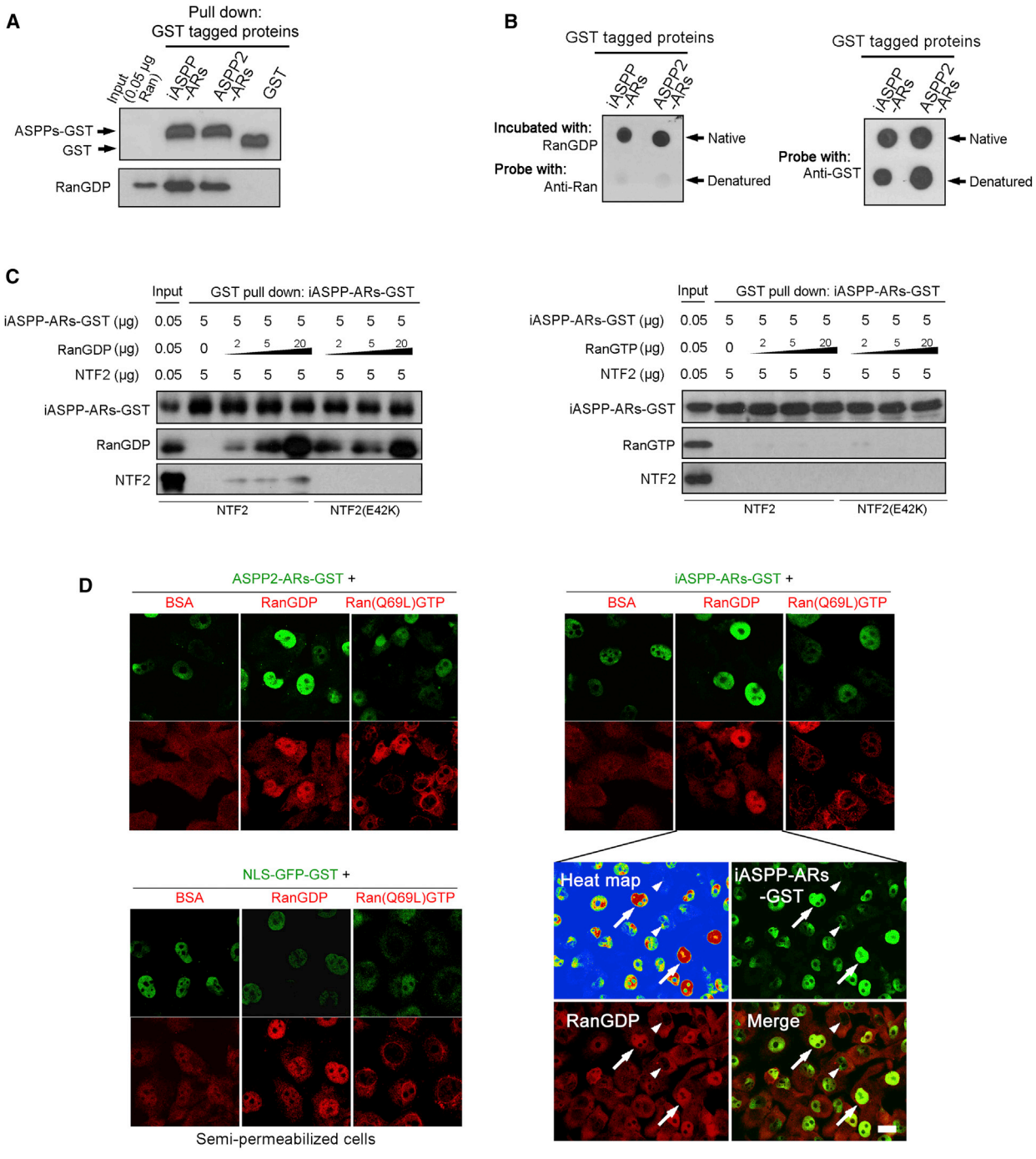

(legend on next page)

more frequently localized in the nucleus than those with two scattered ones (Figure 3C, E-C-K-C versus E-C-C-G).

Structural analysis revealed that a substantial hydrophobic area exists in the C-terminal region of RanGDP (Figure 3D, 176-193, black dot circle), which is either disordered or adopts a drastically different conformation in the RanGTP-bound form. This area is located on the opposite side of the switch II area (NTF2-binding sites, 65-83), supporting the notion that an AR/RanGDP/NTF2 complex can be formed (Figure S3C). To identify the key RanGDP residues that mediate the interaction with hydrophobic AR_{13Hb}, the eight structurally contiguous hydrophobic residues (F176, V177, A181, L182, V187, V188, A192, and L193) in this area were substituted for more hydrophilic arginine residues, either singly or consecutively. While RanGDP single mutants, Ran(V187R)GDP and Ran(V188R)GDP, had minimal impact on binding to IκBα-AR2, RanGDP double-mutant Ran(V187R/V188R)GDP showed a clear defect in binding to IκBα-AR2 (Figure S3D). Similarly, the binding efficiency between Ran(V187R/V188R)GDP and iASPP-ARs is lower than the one between RanGDP and iASPP-ARs (Figure 3E). The binding capacity and dissociation rates of Ran and Ran(V187R/V188R) to GDP or GTP were then analyzed. Similar binding affinities and dissociation rates for GDP or GTP were detected for Ran and Ran(V187R/V188R) (Figures S3E and S3F). Consistent with this, both Ran and Ran(V187R/V188R) were imported into the nucleus in a semipermeable nuclear import assay. Importantly, while RanGDP significantly enhanced the nuclear import efficiency of iASPP-ARs-GST and ASPP2-ARs-GST, the ability of the ARs binding-defect Ran(V187R/V188R)GDP to enhance the nuclear import efficiency of iASPP-ARs-GST and ASPP2-ARs-GST was impaired. Under the same conditions, both RanGDP and Ran(V187R/V188R)GDP had minimal impact on the nuclear import efficiency of NLS-GFP-GST (Figures 3F and S3G and S3H).

Analysis of the computationally docked IκBα-RanGDP-NTF2 complex by HADDOCK suggested that such a ternary complex is feasible, and could position the Ran C-terminal sequence to interact with 2 adjacent ARs at a region centered on the AR_{13}s (Figure S3I) (Chen et al., 2011). These data demonstrate that RanGDP's C-terminal region is required to interact with the AR_{13Hb}, and that AR_{13Hb}s at two consecutive AR stacks form a better RanGDP binding surface than scattered AR_{13Hb}. These results also demonstrate that RanGDP needs to bind ARs to enhance their nuclear import efficiency. RanGDP, but not Ran(V187R/V188R)GDP, selectively enhances the nuclear import efficiency of ARs whereas both RanGDP and Ran(V187R/V188R)GDP had minimal impact on the nuclear import efficiency of NLS-GFP-GST. This further demonstrates that the identified RaDAR pathway is distinct from the NLS/importin-mediated nuclear import pathway.

The Most Common Familial Melanoma Mutation in $p16^{ink4a}$, Occurring at the Second AR_{13}, Confers RanGDP Binding and Nuclear Entry

The cyclin-dependent kinase inhibitor Ink4 family is among the most frequently mutated ARPs in cancer cells, and $p16^{ink4a}$ (p16) is frequently mutated in familial human melanomas. Among the recorded 104 families with familial p16 point mutations, the most frequently occurring event (19.2% frequency) is the M53I mutation (GenoMEL) (Figure S4A) (Goldstein et al., 2006). The AR_{13}s of p16 are defined according to the crystal structure study and, interestingly, M53 is the AR_{13} of p16's second AR (Russo et al., 1998). Another mutation at the AR_{13} of p16's third AR, p16(R87P), has also been detected in melanoma families (1.0% frequency). Most tumor-derived p16 mutants are defective in CDK4 or CDK6 binding and the crystal structure of a CDK6/p16 complex revealed that p16 residues R87 and M53 are located at the interface with CDK4/6 (Russo et al., 1998). As expected, p16(R87P) exhibited a decrease in binding to CDK4 and CDK6. However, p16(M53I) interacted with CDK4 and CDK6 as effectively as wild-type (WT) p16 in vitro and in cell lysates (Figures 4A and 4B).

p16 inhibits cell-cycle entry by preventing cyclin D/CDK4 (or CDK6) from phosphorylating RB. When p16 was induced in U2OS cells (null of endogenous p16), it inhibited RB phosphorylation (Figure 4C) and suppressed cell growth (Figure 4D). Under the same conditions, induced p16(M53I) and p16(R87P) failed to inhibit RB phosphorylation and cell proliferation in U2OS. These results demonstrate that although p16(M53I) binds CDK4/CDK6 as effectively as WT p16, it is functionally defective.

Nuclear cyclin D/CDKs are required to phosphorylate RB and promote cell-cycle entry. Thus, the balance between nuclear cyclin D/CDKs versus p16/CDKs is critical in controlling cell-cycle progression. However, knowledge of how cyclin D, CDK4, and CDK6 enter the nucleus is limited. p16 lacks an identifiable NLS and may enter the nucleus by diffusion, and is detectable in both the cytoplasm and nucleus. However, p16(M53I) is mainly nuclear in vivo in melanocytic lesions of familial melanoma patients (Ghiorzo et al., 2004). Passive transport alone cannot lead to nuclear accumulation (Kim and Elbaum, 2013). In addition, most p16 is complexed with CDK4/6 (resultant 40–66 kDa protein complex) under physiological

Figure 2. ASPP-ARs Directly Bind RanGDP and Form an AR/RanGDP/NTF2 Complex to Mediate Nuclear Entry

(A) 5 μg indicated purified GST-tagged proteins were bound on glutathione beads and incubated in NP40 buffer containing 5 μg/ml purified RanGDP and 2 mg/ml BSA for 2 hr, followed by washes and immunoblotting.

(B) Two microgram of purified ASPP-ARs-GST was spotted on a nitrocellulose membrane and incubated with indicated proteins, followed by probing with shown primary and secondary antibodies. Bottom: (denatured), the ASPP-ARs-GST were incubated in 5 M Urea prior to spotting on the membrane.

(C) Indicated amounts of iASPP-ARs-GST, RanGDP, and NTF2 were mixed in NP40 buffer containing 2 mg/ml BSA for 2 hr. iASPP-ARs-GST was pulled down by glutathione beads, followed by immunoblotting.

(D) FITC (green) labeled ASPP-ARs-GST or NLS-GFP-GST was applied on semipermeable H1299 cells (condition as Figure 1A) in the presence of 0.02 mg/ml PE (red) labeled BSA, RanGDP, or Ran(Q69L)GTP. Arrowheads/arrow: nucleus with low/high levels of PE-Ran. Scale bar, 20 μm.

(E) iASPP-V5 was cotransfected with GFP, Ran-GFP, or Ran(Q69L)-GFP in H1299 for 48 hr and its cellular localization determined using anti-V5 antibody. Scale bar, 20 μm.

See also Figure S2.

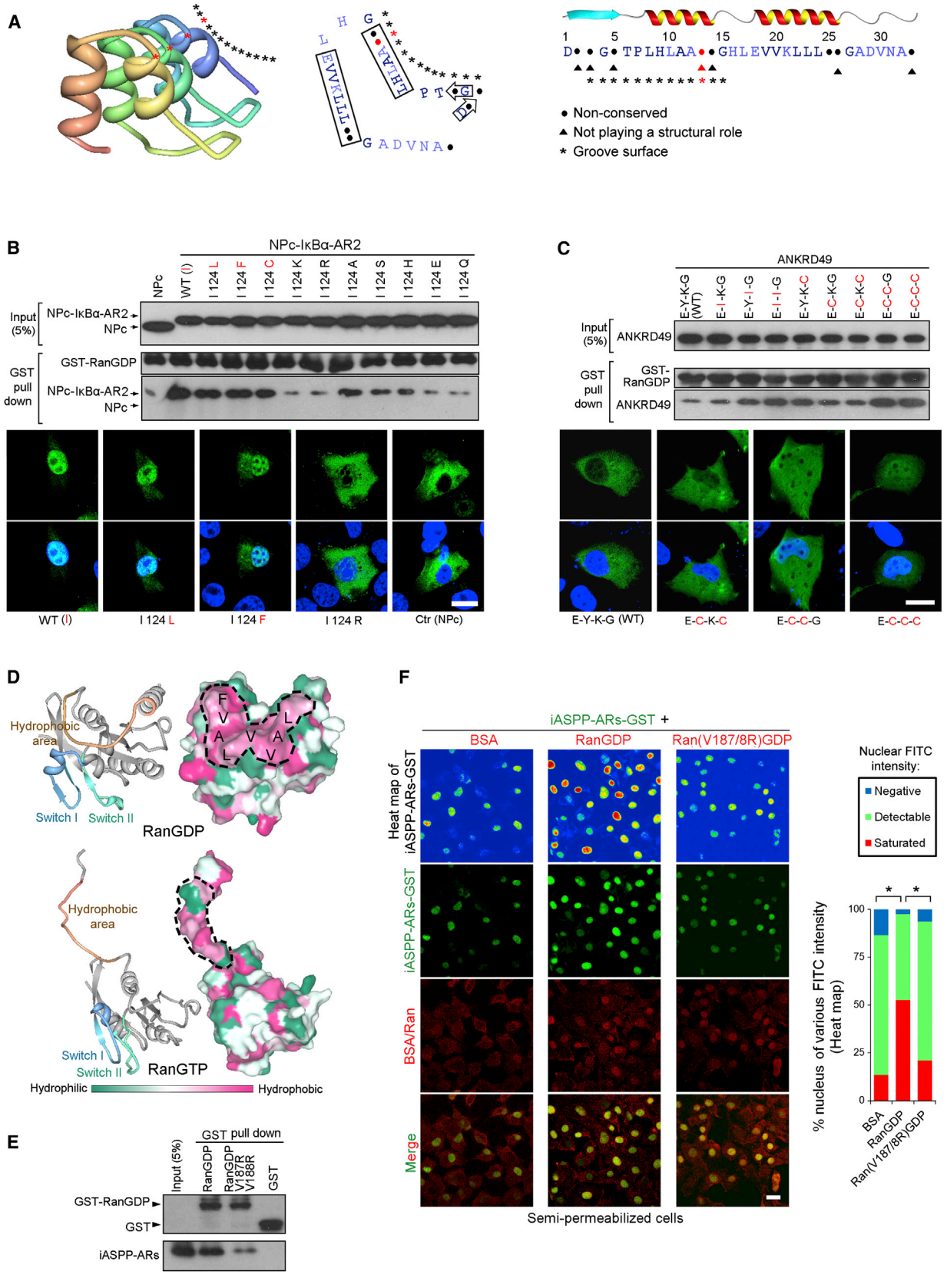

(legend on next page)

conditions (McConnell et al., 1999). Key questions are how p16(M53I) is translocated into the nucleus and why CDK4/6-binding competent nuclear p16(M53I) loses its growth suppressive property.

As M53 and R87 are the AR_{13} of p16's ARs, M53I and R87P mutations may increase p16's RanGDP-binding affinity and nuclear entry. An enhanced nuclear p16(M53I) pool could affect CDK activity by altering CDK or cyclin D levels in the nucleus. This theory was tested by transfecting p16(M53I) or p16(R87P) into IGR39 melanoma cells, which do not express detectable endogenous p16 (Lu et al., 2013). As expected, WT p16 was detected in both the cytoplasm and nucleus, whereas p16(M53I) and p16(R87P) were mainly nuclear (Figure 4E). RanGDP interacted with p16(M53I) and p16(R87P), but not p16 (Figure 4F). Consistent with the notion that RanGDP binding contributes to the enhanced nuclear localization of p16(M53I) and p16(R87P), this effect was largely abrogated by coexpression of p16(M53I) (or p16[R87P]) and Ran(Q69L), a dominant negative Ran mutant (Figure S4B, $p < 0.05$).

It was observed that while most p16-expressing cells expressed cytoplasmic cyclin D1 and CDK4/6, p16(M53I)-expressing U2OS cells tended to express nuclear cyclin D1 and CDK4/6 (Figure 4G, S4C, $p < 0.05$). Notably, lower levels of nuclear cyclin D1 and CDK4/6 were detected in cells expressing p16(R87P), a p16 mutant with reduced CDK4/6-binding capability (Figure S4C). These results suggest that enhanced nuclear accumulation of p16(M53I) via the RaDAR pathway leads to increased nuclear CDK4/6 (Figure S4D, middle). Increased nuclear CDK4/6 may complex with cyclin D1 to retain it in the nucleus and the efficiency of this step may also be affected by an alteration in the affinity of p16(M53I) for CDK4/6. These observations explain how the M53I mutation may cause nuclear entry and functional inactivation, and demonstrate the biological significance of the RaDAR pathway.

RanGDP Binding to AR_{13Hb} Defines a Nuclear Import Pathway

The ability of RanGDP binding to AR_{13Hb} to determine nuclear import was tested using 17 representative ARPs. The 17 constructed ARDs, that have no putative cNLS, were tagged with V5, FLAG, or GFP to generate fusion proteins larger than 30 kDa (Figure S5A top). GST-RanGDP was incubated with cell lysates overexpressing the different ARs in GST pull-down assays. GST-RanGDP interacted with some ARs, and the binding intensities divided them into three groups. iASPP-ARs/RanGDP binding was used to set a reference as 100%. Group 1 ARs (ASPP1, ASPP2, iASPP, IκBα, and TRPV4) bound RanGDP strongly. Group 2 ARs (MYPT1, Tankyrase1, GABPβ1, and ANKRD49) had weak but detectable RanGDP binding. Group 3 ARs (p16, p19, ANKFY1, AnkyrinR, AnkyrinB, AnkyrinG, Notch1, and consensus ARs) had undetectable RanGDP binding (Figure 5A and Figure S5A bottom). Surface plasmon resonance (SPR)-binding assays showed that RanGDP-binding competent group 1 ARPs, iASPP(625-828) and ASPP2(889-1128), specifically bound GST-RanGDP with dissociation constants (Kd values) of 151 nM and 69 nM, respectively (Figure 5B). In contrast, the binding affinities between GST-RanGDP and group 3 ARPs, 6× consensus ARs and AnkyrinR(402-827), were undetectable under the same conditions (Figure S5B), confirming the direct interaction between RanGDP and group 1 ARPs. Interestingly, all group 1 ARs were predominantly nuclear, whereas most of the group 2 and 3 ARs were predominantly cytoplasmic (Figure 5C and S5C).

By examining the hydrophobicity of AR_{13} of the 17 ARDs, a striking association emerged. RanGDP binding to identified hydrophobic AR_{13} (I, L, F, or C) in consecutive ARs was only found in group 1, but not in group 2 or 3, ARPs (Figure 5D). These hydrophobic AR_{13} in nonconsecutive ARs were occasionally found in group 2 and 3 ARs, consistent with those observations made on ANKRD49 (Figure 3C), suggesting that ARPs with hydrophobic AR_{13} in consecutive ARs show more favorable interactions with RanGDP than scattered ones. As ARs are arranged almost linearly, with only a 2–3° counterclockwise angle between neighboring repeats (Michaely et al., 2002), the 3^{rd}–15^{th} residues of each AR form a continuous groove that enables partner protein binding (Figure S5D, star lines). AR_{13} is located on the upper tips of these grooves (red stars), forming an area (circled by black dots, named "13^{th} patch") that is exposed and accessible for RanGDP binding. Interestingly, it was found that group 1 ARPs exhibited an overall hydrophobic "13^{th} patch," while group 2 and 3 ARPs did not (Figure S5E). In group 3, it is well known that cleaved C-terminal Notch1 (Notch1-ICD) is imported into the nucleus via the classical nuclear import pathway (Ranganathan et al., 2011). It is consistent that Notch1-ARs are predominantly cytoplasmic, while Notch-ICD binds importin-α4 and is exclusively

Figure 3. RanGDP Binds Hydrophobic 13^{th} Residue of AR and Mediates Nuclear Import

(A) Left: schematic 3D structure of 3 consensus ARs (PDB: 1N0Q). Middle and right: consensus AR sequence. Position 13 is shown in red.

(B) NPc-IκBα-AR2 mutants (V5 tagged) were transfected into H1299 cells for 48 hr, and GST-RanGDP-binding capacities were determined by GST pull-down assay. In GST pull-down assay, 5 μg purified GST-RanGDP were bound on glutathione beads and incubated in 2 mg/ml H1299 cell lysates (prepared in NP40 buffer) for 2 hr at RT, followed by washes and immunoblotting. Cellular locations of NPc-IκBα-AR2 mutants determined by anti-V5 antibody are shown at bottom. Scale bar, 20 μm.(C) GST-RanGDP-binding capacities and cellular localization of indicated ANKRD49 mutants were determined as for (B).

(D) The fold and surface properties of RanGDP (PDB: 1A2K, chain D) and RanGTP (PDB: 1QBK, chain C) created by Protein Workshop. The substantial hydrophobic surface enclosed within the black dotted lines is composed of residues from the Ran C-terminal region.

(E) Binding between the indicated GST-RanGDP mutants and iASPP-ARs was determined as in (B) using purified GST-RanGDP mutants and H1299 cell lysate expressing iASPP-ARs-V5.

(F) FITC (green) labeled iASPP-ARs-GST was applied on semipermeable H1299 cells (condition as Figure 1A) in the presence of 0.02 mg/ml PE (red) labeled BSA, RanGDP, or Ran(V187R/V188R)GDP. Top: the heat map of iASPP-ARs-GST signal. Bar graph shows the percentage of nuclei with varying FITC intensities according to the iASPP-ARs-GST heat map. Results were collected from two individual experiments and shown as the mean; 100 cells were counted in each panel.

See also Figure S3.

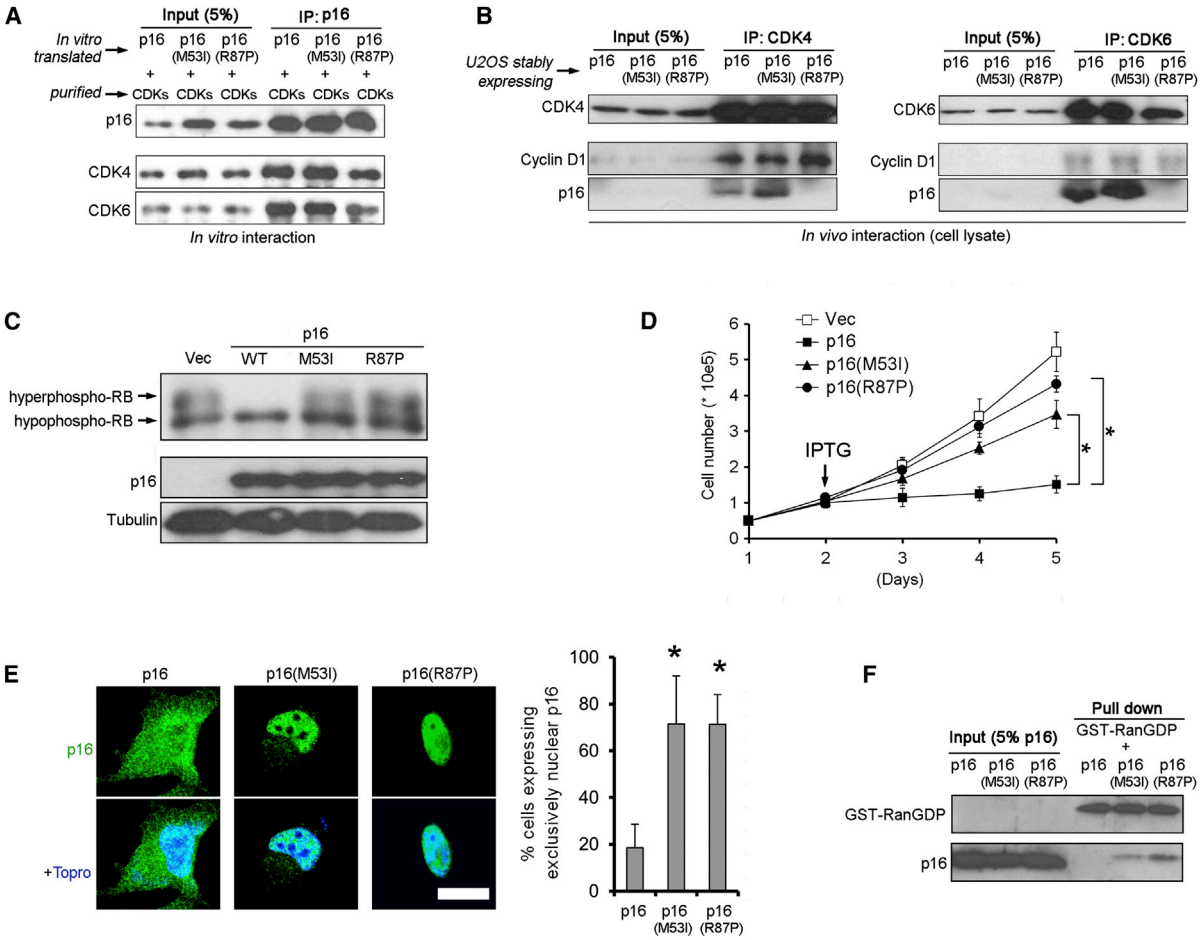

(legend on next page)

nuclear (Figure S5F). The hydrophobic "13th patch" may, therefore, provide access for RanGDP and define the RaDAR pathway.

The Presence of AR_{13Hb} in Two Consecutive ARs Predicts ARP Cellular Localization

Among the 20,254 proteins of the UniProt Human Reviewed Reference Proteins (UHRRP), 256 were identified as ARPs in a homology search. Of the UHRRP proteins, 14,978 are assigned a Cellular Component (C.C.) term by Gene Ontology (GO), and 151 are ARPs (Figure 6A). Interestingly, while 40% of UHRRP are assigned a nuclear C.C. term, an increased proportion (52%) of ARPs are assigned a nuclear C.C. term ($p < 0.01$). Around 50% of >40 kDa ARPs and 58% of >100 kDa ARPs were assigned a nuclear C.C. term, respectively (Figure 6A, shaded area), which is significantly higher than those of non-AR-containing proteins. This suggests a nuclear enrichment of human ARPs that is not caused by passive diffusion of low molecular weight proteins through the NPC.

Nuclear enrichment of ARPs may be mediated by NLS. Using the NLS-searching predictor NucPred (Brameier et al., 2007), we divided the 151 ARPs with GO C.C. terms into three groups according to NLS intensity (Figure S6A). When NLS-containing proteins were excluded from further analysis, the percentage of ARPs assigned a nuclear C.C. term was still higher than those of UHRRP (Figure 6A, $p < 0.01$). This analysis suggests that ARPs can enter the nucleus via an alternative import pathway to the NLS/importin-dependent pathways.

The AR_{13} in individual ARs were identified using an unbiased homology search (Table S1 listing the AR_{13} in 151 ARPs). Fourteen of the 151 ARPs with GO C.C. terms contained I, L, F, or C at the 13th positions of two consecutive ARs (denoted 2× ILFC). Twelve of these 2× ILFC ARPs (86%) were assigned a nuclear C.C. term, while only 49% of the remaining 137 ARPs were assigned a nuclear C.C. term (Figure S6B, $p < 0.05$). When all hydrophobic residues (I, L, F, C, V, M, and A) were considered, 30 of the 151 ARPs with a GO C.C. term (Figure 6B, colorful pies) contained AR_{13Hb} in two consecutive ARs (denoted 2× ILFCVMA, Table S2 listing the 30 2× ILFCVMA ARPs), and 16 of the 105 ARPs without GO C.C. terms (blank pies) contained 2× ILFCVMA. Interestingly, 22 of the 30 2× ILFCVMA ARPs (73%) had a nuclear C.C. term and only 57 of the remaining 121 ARPs (47%) had a nuclear C.C. term (Figure 6B, $p = 0.01$). When all of the 46 2× ILFCVMA ARPs were analyzed, 34 had a nuclear term in either GO or HPA (The Human Protein Atlas), seven were not yet annotated in either database, and only five were assigned a nonnuclear term. Compared with the GO C.C. terms assigned to UHRRP, the "nucleus" term was significantly enriched in the 30 2× ILFCVMA ARPs (Figure 6C, left, $p < 10^{-5}$), while the "cytoplasm" term was enriched in the remaining 121 ARPs without 2× ILFCMV (Figure S6C), suggesting the presence of AR_{13Hb} in two consecutive ARs (2x AR_{13Hb}) may predict ARP cellular localization.

Among the 30 ARPs with 2× ILFCVMA, "transcription factor binding" was the enriched Molecular Function (M.F.) term in GO and the enrichment was statistically significant against GO-assigned UHRRP (Figure 6C, right, $p < 10^{-5}$). The seven proteins assigned this M.F. term were ANKRD42, iASPP, ASPP2, and the NF-κB family members BCL3, IκBα, IκBδ, and NF-κB1. Further analysis of the 30 2× ILFCVMA ARPs revealed that eight were NF-κB family members (Table S2, in yellow), 14 were previously shown to be regulators of NF-κB and/or p53 (in light yellow) and six were assigned an E3 ubiquitin-protein ligase term in UniProt (in blue). No such M.F. term (transcription factor binding) was enriched in the remaining 121 ARPs (Figure S6C, bottom).

In the set of 151 ARPs, the NLS motif tended to associate with 2× ILFCVMA motif-free ARPs (Figure 6D, 23% versus 43%, 40% versus 66%, $p = 0.01$). Notably, all seven ARPs containing both motifs (as shown in Figure 6D) are large proteins (>120 kDa). For large ARPs, both the RaDAR and importin-dependent pathways may contribute to their nuclear localization, suggesting that these two signal motifs generally tend to be mutually exclusive, with either sufficient to mediate ARP nuclear entry.

The presence of AR_{13Hb} was thus used to predict ARP nuclear localization. Four different thresholds were used, based on RanGDP-binding capability. The specificity and sensitivity of these criteria to predict the nuclear localization of 151 GO C.C. term-annotated ARPs was compared to the NLS score-based prediction (Figure 6E; integrated prediction information is given in Table S1). Around 73% of 2× ILFCVMA ARPs had a nuclear C.C. term (specificity), accounting for 28% of the total 79 nuclear ARPs (sensitivity). However, only 59% of NLS-containing ARPs (NucPred score 0.9) had a nuclear C.C. term, and only 25% of the total nuclear ARPs were covered. The same trend was achieved when different thresholds were used. Similar results were also obtained when compared to other NLS-based nuclear localization prediction software including NLStradamus,

Figure 4. The Most Common Familial Melanoma Mutation in $p16^{ink4a}$, Occurring at the Second AR_{13}, Confers $p16^{ink4a}$ Nuclear Accumulation

(A) p16 was prebound on protein G beads and incubated with NP40 buffer containing 2 mg/ml BSA and 5 μg/ml purified CDK4/6-GST for 2 hr. Beads were washed and bound proteins were immunoblotted.

(B) U2OS cells with induced p16 were lysed in NP40 buffer and incubated with protein G beads and 2 μg corresponding CDK4/6 antibody for 2 hr. Beads were washed and bound proteins were immunoblotted.

(C) p16 was induced in U2OS cells in the presence of IPTG for 48 hr, and the RB phosphorylation pattern determined.

(D) p16-inducible U2OS cells were treated with IPTG on day 2 and cell numbers counted on days 3, 4, and 5 (mean ± SD, n = 3, *$p < 0.05$).

(E) Cellular localization of transfected p16 mutants in p16 null IGR39 melanoma cells. Scale bar, 20 μM. Bar graph shows the percentage of cells expressing exclusively nuclear p16 or indicated mutants (mean ± SD, n = 3, *$p < 0.05$).

(F) p16 or indicated mutants were in vitro translated and incubated with 5 μg GST-RanGDP in NP40 buffer, followed by GST pull-down assay using glutathione beads.

(G) Image shows the cellular location of transfected p16 (or p16[M53I]) in U2OS cells. Endogenous CDK4, CDK6, and cyclin D1 (red) were costained with p16 (green), respectively. Scale bar, 20 μm.

See also Figure S4.

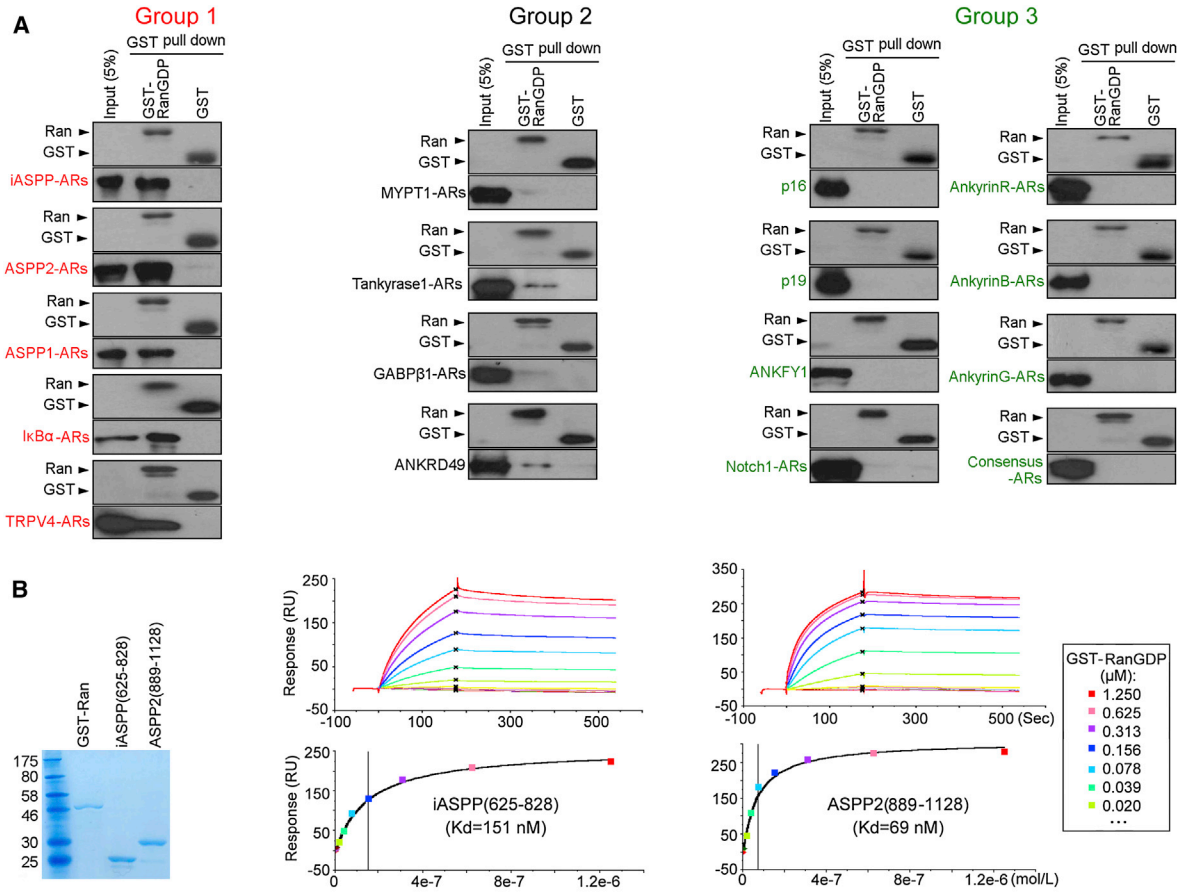

D

17 ARDs	AR13 in each AR	RanGDP binding	Cellular distribution
iASPP-ARDs	L C S	++	N>C
ASPP2-ARDs	L C S	++	N>C
ASPP1-ARDs	L C S	++	N>C
IκBα-ARDs	I I E I D	++	N
TRPV4-ARDs	R L E C I E	++	N
MYPT1-ARDs	S I S A H	+	N>C
Tankyrase1-ARDs	R G S I A R G S S A R A E L G K G S A V K G S Q V	+	N<C
GABPβ1-ARDs	R Q S E D	+	N=C
ANKRD49	E Y K G	+	N<C
p16ink4a	A M R E	–	N=C
p19ink4d	A M R Q Q	–	N=C
ANKFY1	K S Q L M R A W Q R A D S S T Q Q Q M Q M	–	C
Notch1-ARDs	R S R A R	–	N<C
AnkyrinR-ARDs	F R R R K H K Q Q H Q R	–	N.D.
AnkyrinB-ARDs	R K L Q Q R H K R Q H K F R R R K H K Q Q H Q R	–	N<C
AnkyrinG-ARDs	R K L Q Q R H K R Q H K F R R R K H K Q Q H Q R	–	N<C
Consensus-ARDs	R R R R R R	–	N<C

(legend on next page)

predictNLS, PSORT II, LOCtree, and BaCello (data not shown). This analysis demonstrates that the presence of 2× AR_{13Hb} is more specific and sensitive than predictors based on the NLS in predicting the nuclear localization of ARPs.

DISCUSSION

Protein function is dictated by cellular localization. Since the identification of the first NLS in 1984, most nuclear import pathways have been characterized as (centering on) employing importin-cargo interaction-mediated nuclear import pathways. However, these pathways cannot adequately explain how nuclear entry is achieved for the entire proteome, as many of the nuclear proteomic proteins do not have an identifiable NLS. One of the major conceptual challenges is whether a general nuclear import pathway exits that is parallel to the importin-cargo-mediated nuclear import pathway. Our results identify the RaDAR pathway as one such pathway (Figure S6D). Strong and specific binding is necessary for the transport receptor to detect and capture its cargo in the cytoplasm and to maintain a stable complex as it crosses the nuclear pores. Consistent with this, the Kds between monopartite (SV40 NLS) or bipartite (nucleoplasmin) NLS and the importin-α/β complex, measured by SPR, is 35 nM and 48 nM, respectively (Catimel et al., 2001). The Kd between M9 PY-NLS and transportin measured by isothermal titration calorimetry (ITC) is 42 nM (Lee et al., 2006). The Kd between RanGDP and NTF2 is 152 nM by ITC (Chaillan-Huntington et al., 2000). In contrast to the cargo and transport receptor interaction, the binding affinity between the transport complex and FG-Nup is much weaker. A low binding affinity between the transport complex and the NPC may enable rapid attachment and detachment, as a high binding affinity would imply slow off-rates (Stewart, 2007). The observed binding affinities between group 1 ARPs and RanGDP (Kd of 69 and 151 nM) are well-suited for RanGDP to detect and capture ARPs in the cytoplasm, providing strong supporting evidence that the identified RaDAR complex fulfills the requirements of being a novel cargo and transport receptor complex for nuclear import.

Our results also reveal differences between the RaDAR pathway and the nuclear import mechanism reported previously for CapG (Van Impe et al., 2008). First, the binding epitope between the cargo and transport receptor is different. Although CapG directly binds both NTF2 and Ran simultaneously, CapG mainly binds NTF2 to achieve nuclear import while Ran plays a supplementary role by enhancing their binding. CapG binds NTF2 with a Kd of 6,300 nM. The presence of Ran enhances the CapG/NTF2 binding (Kd = 3,800 nM). In contrast, ARPs directly bind RanGDP and complex with NTF2 indirectly via Ran. Moreover, there is a striking difference in the binding affinity between the cargo and transport receptor between CapG/NTF2/Ran versus RaDAR. In the RaDAR pathway, the cargo/receptor binding affinities are 25-55-fold stronger than those of CapG/NTF2/Ran. CapG directly binds Nup62 during NPC crossing, while binding of ARPs and Nup62 was undetectable in this study. It is possible that the previously reported CapG/NTF2/Ran nuclear import pathway may be specific to CapG, whereas the identified RaDAR pathway represents a more general nuclear import pathway.

The RaDAR pathway may explain why some ARPs are located in the nucleus without a detectable NLS. One such example is Tankyrase1. Tankyrase1 belongs to a nuclear protein family, poly(ADP-ribose) polymerase (PARP), and regulates telomere length. While other PARP family members such as PARP1 contain an obvious NLS (Rouleau et al., 2010), Tankyrase1 lacks one and it is unknown how it gains nuclear entry. One possible mechanism is that it piggybacks on NLS-containing proteins (Smith and de Lange, 1999). Alternatively, since Tankyrase1 can bind RanGDP it may use the RaDAR pathway.

The identified RaDAR pathway may provide a molecular explanation for the behavior of numerous ARP mutations in human disease, as demonstrated by the most common familial melanoma founder mutation, p16(M53I). M53I mutation confers p16 RanGDP binding and nuclear enrichment. Nuclear p16(M53I)-expressing cells often coexpress nuclear Cyclin D1 and nuclear CDK4/6. Consistent with the fact that p16(R87P) does not interact with CDK4/6 as efficiently as p16(M53I), nuclear p16(R87P)-expressing cells contain less nuclear Cyclin D1 or nuclear CDK4/6 comparing to p16(M53I)-expressing cells. Therefore, enhanced nuclear p16(M53I), as a result of its uptake via the RaDAR pathway, could lead to increased nuclear CDK4/6 that may retain cyclin D1 in the nucleus and enhance nuclear cyclin D1/CDK's kinase activity to phosphorylate RB and promote cell-cycle entry. Hence, the RaDAR pathway may not only determine the cellular localization of ARPs, but also influence the cellular localization of ARP-interacting proteins.

Finally, unlike the PY-NLS, which is a linear disordered amino acid sequence often located on a protein's surface (Lee et al., 2006), the AR is a highly structured and well-characterized protein motif. The AR code for RaDAR formation is tertiary structure-dependent, and defines an interaction surface (13^{th} patch) for RanGDP binding. This may be part of the reason why the presence of a 2× AR_{13Hb} code for RanGDP binding enabled us to predict nuclear ARPs with high accuracy. Strikingly, detailed analysis of the 30 ARPs that contain 2× AR_{13Hb} revealed three functional clusters. Cluster 1 contains known NF-κB family members, whereas cluster 2 consists of regulators of NF-κB

Figure 5. RanGDP Binding to AR_{13Hb} Defines a Nuclear Import Pathway

(A) Indicated ARs were transfected into H1299 cells and their binding to GST-RanGDP determined in a GST pull-down assay using transfected cell lysates (as Figure 3B).

(B) Purified biotinylated ASPP fragments were immobilized onto a sensor chip coupled with streptavidin, followed by SPR assay. Values of Kd with GST-RanGDP were obtained by nonlinear regression assuming the Langmuir adsorption model. RU, response units. Coomassie blue staining of approximate 1 μg purified proteins is shown.

(C) Cellular localizations of ARs from (A) were determined. Scale bar, 20 μm.

(D) Table lists the RanGDP binding and observed cellular localizations of 17 ARDs derived from (A) and (C). AR_{13} was defined by UniProt.

See also Figure S5.

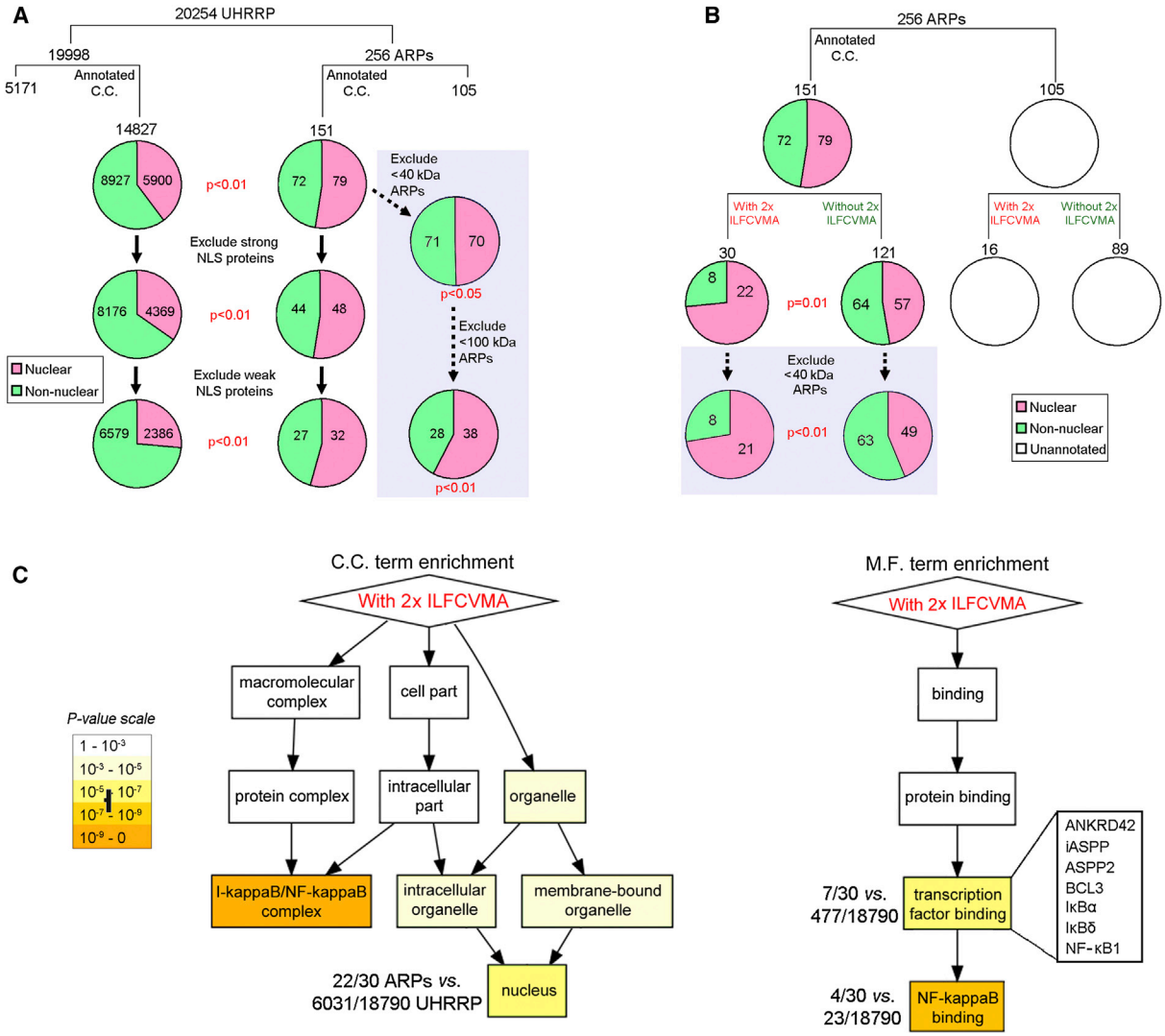

(legend on next page)

and/or p53. The two clusters together account for >70% of the identified 2×x AR_{13Hb} ARPs. The ASPP family proteins were originally identified as binding partners of p53 and p65/RelA. Studies over the past 10 years have established ASPPs as important regulators of p53, p63, and p73 (Bergamaschi et al., 2004). However, much less is known about the biological importance of the ASPP/p65 interaction. The functional interplay between NF-κB and p53 is emerging. Thus, the identification of the RaDAR pathway as a common pathway regulating the nuclear entry of NF-κB family members/regulators and ASPP reveals a new dimension to the crosstalk between NF-κB and p53. Finally, cluster 3 ARPs are assigned an "E3 ubiquitin-protein ligase" term in UniProt. Although the significance of cluster 3 is unknown, it is possible that they may also play a role in regulating NF-κB/p53 signaling, since the stabilities of IκB and p53 are largely regulated by ubiquitin-mediated protein degradation (Brooks and Gu, 2006; Deng et al., 2000). Interestingly, four of them (MIB1, MIB2, ASB9, and FEM1A) are reported to regulate NF-κB's activities (Table S2). Regardless, the remarkably high frequency of 2× AR_{13Hb} ARPs in regulating NF-κB/p53 signaling argues for the importance of the identified RaDAR pathway in diseases such as cancer and inflammation, in which the NF-κB/p53 pathways are deregulated.

Over 250 ARPs are predicted in the human proteome with diverse biological functions, and ARs are one of the most common repeat motifs that mediate protein-protein interactions. The identification of an AR code for RanGDP binding provides a proof of principle that binding specificities of ARs to their interacting proteins may be predetermined by their amino acid sequences. This knowledge will undoubtedly extend our understanding of how ARPs and their interacting proteins function, and will also inform the protein engineering of specific recognition motifs with particular cellular localizations in order to benefit human health.

EXPERIMENTAL PROCEDURES

Computational Protein Sequence Analysis

A multiple protein sequence alignment of ARs was obtained from the Pfam database. Profiles of the alignment were generated using HMMer2. Iterative similarity searches were performed with HMMer2 against the UHRRP database. GO term searches were performed in September, 2013. See Extended Experimental Procedures.

Immunoprecipitation

Cells were lysed in NP40 buffer (50 mM Tris-HCl [pH 8.0], 150 mM NaCl, 1% NP40) with protease inhibitor cocktail. After Sonication and spinning, supernatant was adjusted to a final concentration of 2 mg/ml total protein using NP40 buffer. 400 μl cell lysate was incubated with 20 μl protein G beads and 2 μg corresponding primary antibody for 2 hr at room temperature (RT). Beads were washed four times with NP40 buffer, boiled for 5 min in SDS loading buffer, and used for immunoblotting.

GST Pull-Down

Glutathione beads preincubated with 5 μg purified GST-tagged proteins were incubated in 400 μl NP40 buffer containing 2 mg/ml prepared cell lysate (or NP40 buffer containing 5 μg/ml purified proteins and 2 mg/ml BSA or NP40 buffer containing 10 μl in vitro-translated protein lysate) for 2 hr at RT, followed by washes and immunoblotting.

Ran Nucleotides Loading/Dissociation

A solution of Ran at 20 uM concentration was dialyzed against loading buffer (10 mM HEPES [pH 7.3], 160 mM potassium acetate, 5 mM magnesium acetate, 1 mM DTT) at 4°C overnight (O/N). Dialyzed Ran proteins were incubated with 1 mM of the respective nucleotides in the presence of 15 mM EDTA for 60 min at RT. Magnesium acetate was added to a final concentration of 30 mM.

Protein Fluorescent Labeling and In Vitro Nuclear Import Assay

Ran was loaded with nucleotides immediately prior to experiments. Purified proteins were labeled with FITC or phycoerythrin (PE) using commercially available kits. Digitonin-treated semipermeable cells were incubated in nuclear transport buffer (NIB: 20 mM HEPES [pH 7.3], 110 mM potassium acetate, 5 mM sodium acetate, 2 mM magnesium acetate, 2 mM DTT, 0.5 mM EGTA, and protease inhibitors) with 0.02 mg/ml FITC-labeled substrates, 10 mg/ml H1299 cytosol, and an energy-regenerating mixture (1 mM ATP, 0.1 mM GTP, 5 mM creatine phosphate, and 20 U/ml creatine phosphokinase) at RT for 40 min. Cellular localization of the substrate was determined by direct FITC or PE fluorescence observation with a confocal microscope.

SUPPLEMENTAL INFORMATION

Supplemental Information includes Extended Experimental Procedures, six figures, and two tables and can be found with this article online at http://dx.doi.org/10.1016/j.cell.2014.05.006.

AUTHOR CONTRIBUTIONS

X.L. oversaw the project. M.L. and X.L. conceived and designed the study and wrote the manuscript. M.L., J.Z., S.C., L.S.P. and D.T.S. performed the experiments and J.E., C.P.P. and C.J.S. supervised part of the project. All authors interpreted data and edited the manuscript.

ACKNOWLEDGMENTS

This work was funded by the Ludwig Institute for Cancer Research Ltd. We thank Andrew Wilde, Katrien Van Impe, Paul Clarke, Svitlana Korolchuk, Ming Yang, Vann Bennett, Matthew Cockman, and Mark Hannink for the generous gift of plasmids or proteins. We thank Yvonne Jones for generous access to facilities for protein production. We thank Claire Beveridge and Kimberley Bryon-Dodd for critical reading of the manuscript.

Figure 6. The Presence of 2× AR_{13Hb} Predicts ARP Nuclear Localization

(A) Pie charts show the percentage of UHRRP and ARPs that are assigned with nuclear C.C. terms in GO. Proteins with <40 or 100 kDa (shaded area) or a putative NLS were excluded. p value shows the difference between UHRRP and ARPs.

(B) 151 ARPs with GO C.C. terms and 105 ARPs without GO C.C. terms were divided into two groups according to the occurrence of a 2× ILFCVMA, followed by analysis as (A).

(C) The 151 identified ARPs with a 2× ILFCVMA motif were subjected to C.C. and M.F. enrichment analysis and the significant enrichments were shown (colored). Background: 20254 UHRRP. 18790 proteins from UHRRP were annotated in the GO.

(D) Bar graph shows the occurrence frequency of NLSs in ARPs with/without a 2× ILFCVMA motif.

(E) The specificity and sensitivity of nuclear localization predictions on 151 ARPs according to the occurrence of AR_{13Hb} (red line) or NLS (green line, by NucPred).

See also Figure S6, Table S1, S2.

Received: September 10, 2013
Revised: January 22, 2014
Accepted: March 13, 2014
Published: May 22, 2014

REFERENCES

Adams, R.L., and Wente, S.R. (2013). Uncovering nuclear pore complexity with innovation. Cell *152*, 1218–1221.

Agrawal, N., Frederick, M.J., Pickering, C.R., Bettegowda, C., Chang, K., Li, R.J., Fakhry, C., Xie, T.X., Zhang, J., Wang, J., et al. (2011). Exome sequencing of head and neck squamous cell carcinoma reveals inactivating mutations in NOTCH1. Science *333*, 1154–1157.

Aylon, Y., Ofir-Rosenfeld, Y., Yabuta, N., Lapi, E., Nojima, H., Lu, X., and Oren, M. (2010). The Lats2 tumor suppressor augments p53-mediated apoptosis by promoting the nuclear proapoptotic function of ASPP1. Genes Dev. *24*, 2420–2429.

Bennett, V., and Baines, A.J. (2001). Spectrin and ankyrin-based pathways: metazoan inventions for integrating cells into tissues. Physiol. Rev. *81*, 1353–1392.

Bergamaschi, D., Samuels, Y., Jin, B., Duraisingham, S., Crook, T., and Lu, X. (2004). ASPP1 and ASPP2: common activators of p53 family members. Mol. Cell. Biol. *24*, 1341–1350.

Brameier, M., Krings, A., and MacCallum, R.M. (2007). NucPred—predicting nuclear localization of proteins. Bioinformatics *23*, 1159–1160.

Brooks, C.L., and Gu, W. (2006). p53 ubiquitination: Mdm2 and beyond. Mol. Cell *21*, 307–315.

Catimel, B., Teh, T., Fontes, M.R., Jennings, I.G., Jans, D.A., Howlett, G.J., Nice, E.C., and Kobe, B. (2001). Biophysical characterization of interactions involving importin-alpha during nuclear import. J. Biol. Chem. *276*, 34189–34198.

Chaillan-Huntington, C., Braslavsky, C.V., Kuhlmann, J., and Stewart, M. (2000). Dissecting the interactions between NTF2, RanGDP, and the nucleoporin XFXFG repeats. J. Biol. Chem. *275*, 5874–5879.

Chen, S., Bubeck, D., MacDonald, B.T., Liang, W.X., Mao, J.H., Malinauskas, T., Llorca, O., Aricescu, A.R., Siebold, C., He, X., and Jones, E.Y. (2011). Structural and functional studies of LRP6 ectodomain reveal a platform for Wnt signaling. Dev. Cell *21*, 848–861.

Chook, Y.M., and Süel, K.E. (2011). Nuclear import by karyopherin-βs: recognition and inhibition. Biochim. Biophys. Acta *1813*, 1593–1606.

Cook, A., Bono, F., Jinek, M., and Conti, E. (2007). Structural biology of nucleocytoplasmic transport. Annu. Rev. Biochem. *76*, 647–671.

Deng, L., Wang, C., Spencer, E., Yang, L., Braun, A., You, J., Slaughter, C., Pickart, C., and Chen, Z.J. (2000). Activation of the IkappaB kinase complex by TRAF6 requires a dimeric ubiquitin-conjugating enzyme complex and a unique polyubiquitin chain. Cell *103*, 351–361.

Dreier, B., Honegger, A., Hess, C., Nagy-Davidescu, G., Mittl, P.R., Grütter, M.G., Belousova, N., Mikheeva, G., Krasnykh, V., and Plückthun, A. (2013). Development of a generic adenovirus delivery system based on structure-guided design of bispecific trimeric DARPin adapters. Proc. Natl. Acad. Sci. USA *110*, E869–E877.

Eber, S.W., Gonzalez, J.M., Lux, M.L., Scarpa, A.L., Tse, W.T., Dornwell, M., Herbers, J., Kugler, W., Ozcan, R., Pekrun, A., et al. (1996). Ankyrin-1 mutations are a major cause of dominant and recessive hereditary spherocytosis. Nat. Genet. *13*, 214–218.

Fagotto, F., Glück, U., and Gumbiner, B.M. (1998). Nuclear localization signal-independent and importin/karyopherin-independent nuclear import of beta-catenin. Curr. Biol. *8*, 181–190.

Ghiorzo, P., Villaggio, B., Sementa, A.R., Hansson, J., Platz, A., Nicoló, G., Spina, B., Canepa, M., Palmer, J.M., Hayward, N.K., and Bianchi-Scarrà, G. (2004). Expression and localization of mutant p16 proteins in melanocytic lesions from familial melanoma patients. Hum. Pathol. *35*, 25–33.

Goldstein, A.M., Chan, M., Harland, M., Gillanders, E.M., Hayward, N.K., Avril, M.F., Azizi, E., Bianchi-Scarra, G., Bishop, D.T., Bressac-de Paillerets, B., et al.; Melanoma Genetics Consortium (GenoMEL) (2006). High-risk melanoma susceptibility genes and pancreatic cancer, neural system tumors, and uveal melanoma across GenoMEL. Cancer Res. *66*, 9818–9828.

Görlich, D., and Kutay, U. (1999). Transport between the cell nucleus and the cytoplasm. Annu. Rev. Cell Dev. Biol. *15*, 607–660.

Kim, S., and Elbaum, M. (2013). A simple kinetic model with explicit predictions for nuclear transport. Biophys. J. *105*, 565–569.

Kohl, A., Binz, H.K., Forrer, P., Stumpp, M.T., Plückthun, A., and Grütter, M.G. (2003). Designed to be stable: crystal structure of a consensus ankyrin repeat protein. Proc. Natl. Acad. Sci. USA *100*, 1700–1705.

Kose, S., Furuta, M., and Imamoto, N. (2012). Hikeshi, a nuclear import carrier for Hsp70s, protects cells from heat shock-induced nuclear damage. Cell *149*, 578–589.

Kutay, U., Bischoff, F.R., Kostka, S., Kraft, R., and Görlich, D. (1997). Export of importin alpha from the nucleus is mediated by a specific nuclear transport factor. Cell *90*, 1061–1071.

Lee, B.J., Cansizoglu, A.E., Süel, K.E., Louis, T.H., Zhang, Z., and Chook, Y.M. (2006). Rules for nuclear localization sequence recognition by karyopherin beta 2. Cell *126*, 543–558.

Lu, M., Breyssens, H., Salter, V., Zhong, S., Hu, Y., Baer, C., Ratnayaka, I., Sullivan, A., Brown, N.R., Endicott, J., et al. (2013). Restoring p53 function in human melanoma cells by inhibiting MDM2 and cyclin B1/CDK1-phosphorylated nuclear iASPP. Cancer Cell *23*, 618–633.

McConnell, B.B., Gregory, F.J., Stott, F.J., Hara, E., and Peters, G. (1999). Induced expression of p16(INK4a) inhibits both CDK4- and CDK2-associated kinase activity by reassortment of cyclin-CDK-inhibitor complexes. Mol. Cell. Biol. *19*, 1981–1989.

Melchior, F., Paschal, B., Evans, J., and Gerace, L. (1993). Inhibition of nuclear protein import by nonhydrolyzable analogues of GTP and identification of the small GTPase Ran/TC4 as an essential transport factor. J. Cell Biol. *123*, 1649–1659.

Michaely, P., Tomchick, D.R., Machius, M., and Anderson, R.G. (2002). Crystal structure of a 12 ANK repeat stack from human ankyrinR. EMBO J. *21*, 6387–6396.

Mohler, P.J., Schott, J.J., Gramolini, A.O., Dilly, K.W., Guatimosim, S., duBell, W.H., Song, L.S., Haurogné, K., Kyndt, F., Ali, M.E., et al. (2003). Ankyrin-B mutation causes type 4 long-QT cardiac arrhythmia and sudden cardiac death. Nature *421*, 634–639.

Mohr, D., Frey, S., Fischer, T., Güttler, T., and Görlich, D. (2009). Characterisation of the passive permeability barrier of nuclear pore complexes. EMBO J. *28*, 2541–2553.

Morrison, J., Yang, J.C., Stewart, M., and Neuhaus, D. (2003). Solution NMR study of the interaction between NTF2 and nucleoporin FxFG repeats. J. Mol. Biol. *333*, 587–603.

Notari, M., Hu, Y., Koch, S., Lu, M., Ratnayaka, I., Zhong, S., Baer, C., Pagotto, A., Goldin, R., Salter, V., et al. (2011). Inhibitor of apoptosis-stimulating protein of p53 (iASPP) prevents senescence and is required for epithelial stratification. Proc. Natl. Acad. Sci. USA *108*, 16645–16650.

Ranganathan, P., Weaver, K.L., and Capobianco, A.J. (2011). Notch signalling in solid tumours: a little bit of everything but not all the time. Nat. Rev. Cancer *11*, 338–351.

Ribbeck, K., Lipowsky, G., Kent, H.M., Stewart, M., and Görlich, D. (1998). NTF2 mediates nuclear import of Ran. EMBO J. *17*, 6587–6598.

Rouleau, M., Patel, A., Hendzel, M.J., Kaufmann, S.H., and Poirier, G.G. (2010). PARP inhibition: PARP1 and beyond. Nat. Rev. Cancer *10*, 293–301.

Russo, A.A., Tong, L., Lee, J.O., Jeffrey, P.D., and Pavletich, N.P. (1998). Structural basis for inhibition of the cyclin-dependent kinase Cdk6 by the tumour suppressor p16INK4a. Nature *395*, 237–243.

Sachdev, S., Hoffmann, A., and Hannink, M. (1998). Nuclear localization of IkappaB alpha is mediated by the second ankyrin repeat: the IkappaB alpha

ankyrin repeats define a novel class of cis-acting nuclear import sequences. Mol. Cell. Biol. *18*, 2524–2534.

Samuels-Lev, Y., O'Connor, D.J., Bergamaschi, D., Trigiante, G., Hsieh, J.K., Zhong, S., Campargue, I., Naumovski, L., Crook, T., and Lu, X. (2001). ASPP proteins specifically stimulate the apoptotic function of p53. Mol. Cell *8*, 781–794.

Sedgwick, S.G., and Smerdon, S.J. (1999). The ankyrin repeat: a diversity of interactions on a common structural framework. Trends Biochem. Sci. *24*, 311–316.

Slee, E.A., Gillotin, S., Bergamaschi, D., Royer, C., Llanos, S., Ali, S., Jin, B., Trigiante, G., and Lu, X. (2004). The N-terminus of a novel isoform of human iASPP is required for its cytoplasmic localization. Oncogene *23*, 9007–9016.

Smith, S., and de Lange, T. (1999). Cell cycle dependent localization of the telomeric PARP, tankyrase, to nuclear pore complexes and centrosomes. J. Cell Sci. *112*, 3649–3656.

Sottocornola, R., Royer, C., Vives, V., Tordella, L., Zhong, S., Wang, Y., Ratnayaka, I., Shipman, M., Cheung, A., Gaston-Massuet, C., et al. (2010). ASPP2 binds Par-3 and controls the polarity and proliferation of neural progenitors during CNS development. Dev. Cell *19*, 126–137.

Stewart, M. (2007). Molecular mechanism of the nuclear protein import cycle. Nat. Rev. Mol. Cell Biol. *8*, 195–208.

Van Impe, K., Hubert, T., De Corte, V., Vanloo, B., Boucherie, C., Vandekerckhove, J., and Gettemans, J. (2008). A new role for nuclear transport factor 2 and Ran: nuclear import of CapG. Traffic *9*, 695–707.

Vigneron, A.M., Ludwig, R.L., and Vousden, K.H. (2010). Cytoplasmic ASPP1 inhibits apoptosis through the control of YAP. Genes Dev. *24*, 2430–2439.

Vives, V., Su, J., Zhong, S., Ratnayaka, I., Slee, E., Goldin, R., and Lu, X. (2006). ASPP2 is a haploinsufficient tumor suppressor that cooperates with p53 to suppress tumor growth. Genes Dev. *20*, 1262–1267.

Wang, Y., Godin-Heymann, N., Dan Wang, X., Bergamaschi, D., Llanos, S., and Lu, X. (2013). ASPP1 and ASPP2 bind active RAS, potentiate RAS signalling and enhance p53 activity in cancer cells. Cell Death Differ. *20*, 525–534.

Weis, K. (2003). Regulating access to the genome: nucleocytoplasmic transport throughout the cell cycle. Cell *112*, 441–451.

Yang, J.P., Hori, M., Sanda, T., and Okamoto, T. (1999). Identification of a novel inhibitor of nuclear factor-kappaB, RelA-associated inhibitor. J. Biol. Chem. *274*, 15662–15670.